

# Co-expression and function of head-to-head NLR gene pair Pik-H4

Fengwei Gu<sup>1</sup>, Huabin Xie<sup>1</sup>, Qiwei Huang<sup>1</sup>, Shang Gao<sup>1</sup>, Tao Guo<sup>1</sup>, Jiafeng Wang<sup>1</sup>, and Hui Wang<sup>1</sup>

<sup>1</sup>South China Agricultural University

September 15, 2023

## Abstract

Nucleotide-binding, leucine-rich repeat (NLR) genes play a pivotal role in shaping plant effector-triggered immunity in response to pathogen invasions. However, the mechanisms governing the expression and behavior of NLRs, particularly in the context of head-to-head NLR gene pairs, in the presence of pathogens, remain uncovered. In this study, we dissected the *Pik-H4* promoter (P *Pik-H4*) at the TATA boxes and conducted an in-depth investigation into split promoter activity using Agro-infiltration assays. The segments spanning 593-1232 bp and 2016-2492 bp (starting from -1 bp of *Pik1-H4*) within P *Pik-H4* emerged as core regions for expressing *Pik1-H4* and *Pik2-H4* respectively. Nevertheless, merging these two core fragments failed to recover the promoter activity in both directions. Employing Gus staining, promoter activity assays and qRT-PCR, we unveiled the co-expression of *Pik1-H4* and *Pik2-H4* throughout the whole plant. Additionally, in the presence of the rice blast fungus, their co-amplification was observed in leaves and leaf sheaths. Strikingly, *Pik-H4* exhibited heightened expression within vascular bundles. Moreover, perturbing the *Pik1-H4* and *Pik2-H4* co-expression relationship via overexpression in rice or *Nicotiana* did not disrupt the immune response. Upon infection, the singleton *Pik1-H4* localized within vesicles, while *Pik2-H4* predominantly occupied the nucleus within leaf sheath cells. Transcriptome analysis highlighted *Pik-H4*-mediated resistance triggering a transcriptome reprogramming between 12 and 24 hours post-inoculation. Notably, overexpression of *Pik1-H4* or *Pik2-H4* enriches various pathways compared to the *Pik-H4* Lijiangheitanxingu near-isogenic lines. In summary, these findings unravel the intricate dynamics of co-expression and singular functionality within NLR bidirectional gene pairs upon pathogen invasion.

## Introduction

Plants defend against pathogens through effector-triggered immunity (ETI) with Resistance (R) proteins recognition of Avirulence (Avr) proteins. Most *R* genes belong to the NLRs family. According to the number of functioning proteins, NLRs can be divided into singletons and pairs. The NLR singletons recognize and/or interact with Avr, resulting in hypersensitive response (HR). The RPP1, ROQ1, and Sr35 directly interact with corresponding effectors and form resistosomes (Ma *et al.*, 2020; Martin *et al.*, 2020; Zhao *et al.*, 2022). Rice R proteins Pi-ta and Pi54 also directly recognize Avr-Pita and Avr-Pi54 respectively (Jia *et al.*, 2000; Ray *et al.*, 2016). In the case of indirect recognition of effectors, one of the most apparent mechanisms is *Arabidopsis* Coiled-coil type NLR (CNL) protein HOPZ-ACTIVATED RESISTANCE 1 (ZAR1). After pathogen infection, ZAR1 is pentameric to a resistosome together with resistance-related kinase 1 (RKS1) and PBS1-like protein 2 (PBL2) (Wang *et al.*, 2019). PBL2 acts as a “decoy” (Wang *et al.*, 2015) and the ZAR1-RKS1-PBL2 resistosome exhibits a plasma membrane localization, function as a Ca<sup>2+</sup> channel, and trigger HR (Bi *et al.*, 2021). After interacting with AVRrpm1 or AVRb, the phosphorylated RIN4 acts as a “guard”, activating the *Arabidopsis* CNL RPM1 and resulting in cell death (Mackey *et al.*, 2002). Upon infection, AvrPib competitively binds to the “protector” of Pib, OsSH3P2, and releases Pib from the OsSH3P2-Pib complex, leading to Pib activation (Xie *et al.*, 2022).

The NLR pairs members play different roles in the integrative decoy model (Cesari, Bernoux, *et al.*, 2014). The one that recognizes Avr functions as a “sensor” and the other NLR that causes HR and downstream

signaling is called a “helper”. As a typical example, the rice CNL pair member RGA5 directly binds to AvrPia, and RGA4 triggers HR (Cesari, Kanzaki, *et al.*, 2014). In contrast, the PigmR/PigmS pair differs from the decoy model. PigmR recognizes the effector and induces HR, while PigmS inhibits cell death (Deng *et al.*, 2017). In addition, *PigmR* and *PigmS* display low expression levels in all tissues except that *PigmS* shows a high transcription activity in panicles and pollens. Some NLR pair members are head-to-head (H2H) construction in chromosomes with an interval of a bidirectional promoter (BDP). Bidirectional genes (BDGs) occur widely in nature. In *Arabidopsis* and rice, 5763 and 8742 genes are organized in BDG architectures (Krom and Ramakrishna, 2008). Since sharing transcription factor binding sites and *cis* elements through BDPs, the BDGs are strongly co-regulated and participated in similar pathways (Williams and Bowles, 2004). The *Arabidopsis* TNL pairs RPS4/RRS1 and CHS1/SOC3 are organized in a BDP manner and spaced with a ~300 bp promoter region. The PRS4/RRS1 complex is necessary for recognizing the AvrRps4 and Pop2 (Williams *et al.*, 2014). Expression of *SOC3* is promoted in the *CHS1* mutant, suggesting that self-regulation through the promoter region of *CHS1* /*SOC3* and the CHS1/SOC3 complex is involved in autoimmunity (Zhang *et al.*, 2017). The only known NLR BDGs in rice are *Pik* genes, and 11 of them are reported. The HR assays of *Pikh* (Zhai *et al.*, 2014) and *Pikp* (Zdrzałek *et al.*, 2020a) indicate that the two members of *Pik* genes are required for recognition of AvrPik and cell death. The co-function of the NLR gene pair requires regulation and coordination in transcription and protein levels. In rice, most of the NLRs are allelic genes of the model species Nipponbare (Nip). The sequence variation of the allelic NLRs makes RNA-seq-based expression pattern analysis difficult. For example, the coding sequences and promoter regions of *Pikh1* /*Pikh2* and the Nipponbare *LOC\_Os11g46200* /*LOC\_Os11g46210* are apparently different. Consequently, the expression pattern and relation of NLRs, especially the NLR pairs, are still unclear.

The CNL gene pair *Pik-H4* is a synonymous mutation of *Pikh* and is resistant to rice blast fungus (Xiao *et al.*, 2011). A homeodomain transcription factor OsBIHD1 is found to interact with *Pik1-H4* and is required to *Pik-H4* induced ETI through regulation of the brassinosteroid-ethylene pathway (Liu *et al.*, 2017). We report that the NLR gene pair *Pik1-H4* and *Pik2-H4* are positively co-expressed in all tissues, highly expressed in vascular bundles, including mesophyll cells and vascular cells, and induced by rice blast fungus through a bidirectional promoter. Overexpressing *Pik1-H4* or *Pik2-H4* promotes the transcription levels of the counterpart *Pik-H4* and does not affect the resistance to rice blast. Singleton *Pik1-H4* and *Pik2-H4* display vesicles and nucleus location respectively during infection, pathway analysis shows that *Pik-H4* mediated immunity is involved in transcription reprogramming and *Pik-H4* singleton functions in various pathways.

## Results

### The characterization of *Pik-H4* promoter

The *Pik* genes, such as *Pik-H4* (Figure 1A), consist of two adjacent and H2H NLRs sharing a promoter region. The promoter region of *Pik-H4* ( $P_{Pik-H4}$ ) was cloned and aligned to that of *Pik-Nip* and *Pikh* (Figure S1). The sequence similarity of  $P_{Pik-H4}$  (2492 bp) and  $P_{Pikh}$  (2542 bp) is 97.44%, and the major sequence differences are located between 1010 bp to 1400 bp of  $P_{Pik-H4}$ , which results in lacking 8 TFBSs compared to  $P_{Pikh}$ .  $P_{Pik-H4}$  and  $P_{Pik-Nip}$  (1099 bp) only share 25.41% similarity, and the promoter sequences of the *Pik-1* direction are highly dissimilar. Interestingly, there are two types of promoter length of available promoter sequences of reported *Pik* genes. *Pik\**, *Pi1*, *Pik-h*, and *Pik-m* promoter regions are 2542 bp in length, while those of *Pi7*, *Pik-H4*, and *Pikp* are approximately 2492 bp. All these promoters are highly conserved even though these *Pik* genes were cloned from different donors (Table S1). Then, the functional motifs of  $P_{Pik-H4}$  were detected (Figure 1B). Ten putative TATA boxes were predicted in  $P_{Pik-H4}$ , and 3 of them were bidirectional TATA boxes. The bidirectional TATA box (5'-TATATAT-3') confers bidirectional transcriptional activity and is highly active (Xu *et al.*, 1991). Therefore, the bidirectional TATA box may enable the  $P_{Pik-H4}$  transcript flanking genes. Besides, TFBSs of well-known immunity-related TFs (ERF, WRKY and Dof) were also found in  $P_{Pik-H4}$ , indicating the pathogen-induced possibility of *Pik-H4*.

### Functional analysis of *Pik-H4* promoter

To identify the crucial region of  $P_{Pik-H4}$ ,  $P_{Pik-H4}$  was fused with  $RFP(Pik_1-H4)$  direction) and  $GFP(Pik_2-H4)$  direction) for further study (Figure S2A). These constructs were subsequently introduced into rice protoplasts and tobacco mesophyll cells via plasmid transformation, and the bidirectional promoter activity was observed in both cell types (Figure S2B). Interestingly, the fluorescence intensities of RFP and GFP exhibited synchronized trends and intensities (Figure S2C). Consequently, we focused on conducting promoter activity assays in tobacco mesophyll cells for further investigations.

Given the essential role of the TATA box in eukaryotic RNA polymerase function and transcription specificity, the  $P_{Pik-H4}$  was split according to the position of TATA boxes. In the  $Pik_1-H4$  direction, the recovery of RFP expression to native promoter (NP) levels occurred until the 7<sup>th</sup> TATA box (1-7T) was included (Figure S2D), indicating the criticality of the 593-1232 bp region for  $Pik_1-H4$  transcription. As the following promoter fragments were added, the promoter activity towards  $Pik_1-H4$  direction decreased, suggesting that the *cis* elements in the following region might negatively regulate  $Pik_1-H4$  expression. Interestingly, all split promoters with no transcription start site (TSS) drove GFP expression at levels similar to the NP.

In the direction of  $Pik_2-H4$ , the 2-1T sequence (2016-2492 bp) was sufficient to restore the  $P_{Pik-H4}$  activity towards  $Pik_2-H4$  direction (Figure S2I). The region spanning from the 5<sup>th</sup> to the 10<sup>th</sup> TATA box upstream  $Pik_2-H4$  enhanced the GFP expression, suggesting a positive regulatory role in  $Pik_2-H4$  transcription. Notably, this region overlapped with the critical sequence of  $Pik_1-H4$ , establishing  $P_{Pik-H4}$  as a bidirectional promoter configuration. In summary, the 593-1232 bp and 2016-2492 bp of  $P_{Pik-H4}$  were core regions for  $Pik_1-H4$  and  $Pik_2-H4$  expression respectively.

Considering the bidirectional manner and examination of the core promoter region of  $P_{Pik-H4}$ , a series of synthetic bidirectional promoters were constructed based on  $P_{Pik-H4}$ . Surprisingly, while B1, B2, and B4 promoters failed to restore GFP expression levels (Figure 2C), the B3 promoter, comprising the core promoter regions of both  $Pik_1-H4$  and  $Pik_2-H4$ , augmented the GFP signal. Our findings underscore the complexity of regulatory interactions among distinct *cis* elements within the promoter region, particularly when integrating two directional core regions.

A symmetric integrated TATA box, comprising two bidirectional TATA boxes, was identified within  $P_{Pik-H4}$ , prompting a functional analysis. Firstly, the 100 bp fragment including three bidirectional TATA boxes (Figure 2B, BT1) conferred promoter activity in both orientations and this transcriptional activity was recovered to NP levels in the presence of TSSs of the downstream genes (BT2). Notably, the loss of function of the integrated bidirectional TATA box by mutating it from 5'-TATATATA-3' to 5'-AAAAAAAA-3' (M1) significantly compromised promoter activity in both directions, while the normal bidirectional TATA box (M2, M3) had comparatively milder effects on bidirectional promoter activity. Modifying the regular TATA box into the integrated TATA box (M4, M5) demonstrated that the promoter activity towards the  $Pik_2-H4$  direction increased as the integrated TATA box shifted, while the activity of the opposite orientation remained intact. This suggests that the function of the integrated bidirectional TATA box in the  $Pik_2-H4$  direction may be position-dependent within the  $Pik-H4$  promoter region. Our findings were consistent with a previous report that the symmetry 5'-TATATATA-3' is highly active in both directions (Xu, Thali and Schaffner, 1991).

### ***Pik<sub>1</sub>-H<sub>4</sub>* and *Pik<sub>2</sub>-H<sub>4</sub>* co-express in planta**

The expression patterns of BDGs can be classified as co-regulated, anti-regulated or with one direction exclusively regulated (Trinklein *et al.*, 2004). Given the cooperative function of  $Pik_1-H4$  and  $Pik_2-H4$ , it is logical to infer that the  $Pik-H4$  gene pair is co-regulated. To validate this hypothesis,  $P_{Pik_1-H4}::GUS$  /Nip,  $P_{Pik_2-H4}::GUS$  /Nip and  $RFP::P_{Pik-H4}::GFP$  /Nip plants were generated to examine tissue specificity and promoter activity of  $Pik-H4$ . As shown in Figure 3A and Figure S3A,  $P_{Pik-H4}$  displayed activity in both directions in roots, stems, leaf sheaths, leaves, spikelets, and seeds in both GUS staining assay and fluorescent plants, exhibiting constitutive expression patterns. Detecting the fluorescence intensity of RFP and GFP and relative expression levels of  $Pik-H4$  in  $Pik-H4$  Lijiangheituanxingu (LTH) near-isogenic lines (NILs, hereafter,  $Pik-H4$  NILs) showed similar expression trends of  $Pik-H4$  (Figure 3B, 3D). In accordance with the

tobacco filtration assay, the activity of  $P_{Pik1-H4}$  was stronger than  $P_{Pik2-H4}$ . Employing the Pearson's correlation test, the fluorescence intensity, representing the transcription levels of  $Pik1-H4$  and  $Pik2-H4$ , demonstrated a significantly positive co-regulation *in planta* (Figure 3C) and across all tissues (Figure S3B-G). In addition, RFP and GFP signals were particularly robust within vascular bundles in roots, stems, leaf sheaths, and leaves, revealing high  $P_{Pik-H4}$  activity in vascular bundles compared to mesophyll (Figure 3E). Zooming into the cellular level (Figure 3F), the  $Pik-H4$  expression patterns were also measured. Since the leaf sheaths from rice seedlings are thin enough for laser confocal microscopy, we used leaf sheaths for further research. The transcription activity of  $P_{Pik-H4}$  in both directions exhibited a linear correlation in both mesophyll cells (Figure 3G) and vascular cells (Figure 3H) in leaf sheaths. Importantly, the fluorescence intensity of  $P_{Pik-H4}$  was higher in vascular cells (Figure 3I), aligning with the observed trends at the tissue level.

### Rice blast fungus up-regulates the expression of $Pik-H4$

As a resistant gene pair,  $Pik1-H4$  collaborates with  $Pik2-H4$  to participate in rice blast immunity. The presence of W-boxes within the  $P_{Pik-H4}$ , which has been documented to confer promoter responsiveness to fungal or bacterial infections (In *et al.*, 2020), suggests a potential pathogen-induced expression mechanism for  $Pik-H4$ . To identify whether  $Pik-H4$  responds to rice blast fungus, the  $Pik-H4$  NILs leaves were spray inoculated with rice blast fungus carrying AvrPik-E. We found that the  $Pik-H4$  expression levels peaked at 24 hours post-inoculation (hpi) through qRT-PCR analysis (Figure S4A, C), a pattern distinct from the mock treatment (Figure S4B). Notably, this peak coincided with the onset of *M. oryzae* invasion, wherein the penetration peg of the fungus invades rice cells around 24 hpi, followed by the subsequent spread of invasive hyphae between cells (Yan and Talbot, 2016). The temporal alignment of  $Pik-H4$  expression peak with *M. oryzae* invasion highlights its up-regulation at the initiation of ETI.

Since Nip is infectious to AvrPik-E, the  $RFP::P_{Pik-H4}::GFP$  /Nip plants were also inoculated and observed *in planta*. Visible lesion areas emerged on 2 days post-inoculation (dpi) in leaves, and our observations continued as these lesions evolved. As the lesions expanded, the leaf mesophyll became increasingly transparent, enabling laser penetration. As a result, fluorescence intensity data from 4 dpi onward was not collected for this study. The  $P_{Pik-H4}$  activity was measured from the lesion area to the peripheral area along the dotted line in Figure 4A. Within the lesion area, the promoter activity of  $Pik1-H4$  and  $Pik2-H4$  was lower than the average levels but rose at the edge of the lesion (Figure 4B). The RFP signal was higher than the average levels of leaves from the lesion edge to the lesion peripheral region while the GFP signal dropped to the normal state. These findings suggest that  $Pik-H4$  is responsive to rice blast fungus and a putative signaling cascade operates from the lesion area to its periphery. Similar trends were observed at the lesion edge as the lesion expanded in the following days post-inoculation (Data not shown). We observed the promoter activity changes of *M. oryzae* at the biotrophic and necrotrophic stages within vascular bundles (Figure 4C). During the early stage of hypha growth,  $Pik-H4$  displayed no responsiveness (Figure 4D). However, as the hyphae advanced along the vascular bundles,  $P_{Pik-H4}$  activity exhibited up-regulation. Conversely, at the distal end of lesions by 4 dpi, the transcription levels of  $P_{Pik-H4}$  demonstrated no significant difference compared to the mock treatment. Interestingly, the fluorescence intensity of spreading hyphae showed no difference between the hyphal region and its surroundings, while at the biotrophic stage, the intensity was significantly higher than the peripheral area (Figure 4E). As for cell scale, the activity of  $P_{Pik-H4}$  in both mesophyll cells and vascular cells markedly increased upon the appearance of *M. oryzae* (Figure 4F-I), although the linear correlation between  $Pik1-H4$  and  $Pik2-H4$  promoter activity was lost (Figure 4J, K). Notably, no discernible  $P_{Pik-H4}$  activity difference was observed in cells harboring *M. oryzae* spores or hyphae and their adjacent cells (Figure S4G).

Given that the  $Pik-H4$  gene pair demonstrated co-expression in various tissues, rice blast was inoculated in leaf sheaths for  $P_{Pik-H4}$  activity analysis. In  $Pik-H4$  NILs,  $Pik-H4$  conferred rice blast resistance in leaf sheaths (Figure S4D).  $P_{Pik-H4}$  exhibited responsiveness to the rice blast infection, leading to the up-regulation of  $Pik-H4$  in leaf sheaths at 24 hpi in contrast to the mock treatment (Figure S4E, F). Taken together, the  $Pik-H4$  gene pair was rice blast inducible.

## Disequilibration of *Pik-H4* expression did not affect rice blast resistance

The *Pik* gene pairs trigger HR together facing Avr and form a complex (Zdrzałek et al., 2020a). Considering the co-regulation of the *Pik-H4* gene pair via the BDP, we investigated whether the disequilibration of *Pik-H4* expression had any influence on rice blast resistance. Remarkably, the overexpression of either *Pik<sub>1</sub>-H4* or *Pik<sub>2</sub>-H4* in LTH did not confer disease resistance (Figure 5A-C). Conversely, within *Pik-H4* NILs, overexpression of either *Pik<sub>1</sub>-H4* or *Pik<sub>2</sub>-H4* sustained rice blast resistance. Interestingly, overexpression of either *Pik-H4* in LTH led to an enhancement in the expression of the other *Pik* gene in LTH (Figure 5D). The relative expression levels analysis showed overexpressing one of the *Pik-H4* in *Pik-H4* NILs up-regulated the counterpart (Figure 5E). This intriguing regulatory relationship was successfully replicated in tobacco, yielding analogous outcomes (Figure 5F). These findings collectively suggest that, facilitated by the  $P_{Pik-H4}$ , the expression levels of *Pik-H4* are self- and co-regulated. To eliminate the innate regulation of *Pik-H4* in rice, agroinfiltrations of different ratios of *Pik-H4* with *35S* promoter were performed in tobacco (Figure 5G). At the protein level, combinations of *Pik<sub>1</sub>-H4* and *Pik<sub>2</sub>-H4* in 1:1, 1:2, or 2:1 ratios failed to induce HR in the absence of AvrPik-E. However, upon the introduction of AvrPik-E, these combinations exhibited activity in ion leakage assays, with similar conductivity levels recorded at 3 dpi. These results suggested that altering the disequilibration of *Pik-H4* in protein levels did not compromise rice blast resistance.

## Subcellular localization of *Pik<sub>1</sub>-H4* and *Pik<sub>2</sub>-H4* in planta

As NLR pairs, *Pik<sub>1</sub>-H4* and *Pik<sub>2</sub>-H4* collaborate to counter rice blast, invoking HR. In the previous study, we found that *Pik-H4* maintained some expression levels and was blast-induced. To clarify how *Pik-H4* changes between the resting and active stages, our focus turned to observing the subcellular localization of *Pik<sub>1</sub>-H4* and *Pik<sub>2</sub>-H4* singletons or as a pair within leaf sheaths of LTH or *Pik-H4* NILs plants. Interestingly, *Pik<sub>1</sub>-H4-GFP* (Figure 6A, B) and *Pik<sub>2</sub>-H4-GFP* (Figure 6E, F) exhibited varying subcellular localization patterns across different cells. *Pik<sub>1</sub>-H4-GFP* and *Pik<sub>2</sub>-H4-GFP* were observed in the plasma membrane and cytoplasm, with the GFP signals partially coinciding. In OE-*Pik<sub>1</sub>-H4-GFP* /LTH plants, *Pik<sub>1</sub>-H4-GFP* localization extended to the nucleus and vesicle-like particles (Figure 6C), while the *Pik<sub>2</sub>-H4-GFP* singleton predominantly resided within the nucleus. Upon *M. oryzae* invasion of leaf sheaths, *Pik<sub>1</sub>-H4-GFP* relocated to vesicles (Figure 6D), whereas *Pik<sub>2</sub>-H4-GFP* translocated to the nucleus (Figure 6H). Notably, as a sensor, *Pik<sub>1</sub>-H4* singleton may be transported towards *M. oryzae* via vesicles (Figure S5A, B). Our observations revealed *Pik<sub>1</sub>-H4* within numerous minute vesicles (Figure S5C-E) in cells neighboring blast-invaded or normal cells. These findings suggest that *Pik<sub>1</sub>-H4* plays a vital role in recognizing Avr via vesicle transportation, possibly originating from smaller particles in healthier cells and converging into larger vesicles in the presence of rice blast fungus.

Upon overexpression of *Pik<sub>1</sub>-H4* or *Pik<sub>2</sub>-H4* in *Pik-H4* NILs, their subcellular localization was similar to *Pik-H4* singletons in the absence of rice blast fungus (Figure 6I, K), with fewer instances of *Pik<sub>1</sub>-H4-GFP* residing in vesicles. Given the resistance of *Pik-H4* NILs against rice blast, we did not find severe invasion but only several cells with a single spore or short hypha (Figure 6J, L). The appearance of *M. oryzae* significantly attenuated the *Pik<sub>1</sub>-H4-GFP* or *Pik<sub>2</sub>-H4-GFP* and chlorophyll signals in cells inhabited by the fungus and their neighboring cells, indicative of cell death. Although the GFP signals were weak, the *Pik-H4* were mainly found in the membrane or cytoplasm. Interestingly, *Pik<sub>1</sub>-H4* and *Pik<sub>2</sub>-H4* were found in chloroplasts with weak GFP signals (Figure S6A-H) in planta.

## Pathways analysis of *Pik-H4* as singleton or pair

To gain insights into the functional pathways governed by *Pik-H4* as either a singleton or a pair, we conducted transcriptome analyses of LTH and *Pik-H4* NILs exposed to *M. oryzae*, as well as of LTH overexpressing *Pik<sub>1</sub>-H4* or *Pik<sub>2</sub>-H4*. Notably, as both *Pik<sub>1</sub>-H4* and *Pik<sub>2</sub>-H4* were located within the nucleus, we focused on identifying changes in the transcriptomes of these samples through RNA-seq. The data's quality and reproducibility were validated through Pearson correlation analysis of R values among replication groups, indicating robust and consistent results (Figure S7A-J). Investigation revealed that, at 12 hpi, 86 genes were significantly up-regulated (Filtered *Pik-H4* NILs mock and LTH at corresponding hpi,

$P < 0.01$ ,  $|\log_2 \text{Foldchange}| \geq 2$ , the same as below), while 26 genes were significantly down-regulated. At 24 hpi, the numbers were 268 up-regulated and 126 down-regulated genes (Figure 7A). Considering that *M. oryzae* penetration typically occurs around 24 hpi (Li et al., 2023; Yan and Talbot, 2016), these findings suggest that *Pik-H4*-mediated resistance induces transcriptome reprogramming between 12 and 24 hpi post *M. oryzae* treatment. Through gene ontology (GO) pathway enrichment analysis of up- or down-regulated genes (Figure 7B, C), we found that, at 12 hpi, the predominant up-regulated GO pathways encompassed chloroplast-related molecules such as heme and tetrapyrrole binding, alongside enzymatic activities such as catalytic and oxidoreductase functions. In contrast, down-regulated genes were significantly related to chloroplast-related pathways. At 24 hpi, there was a conspicuous shift towards chloroplast-related pathways for up-regulated genes, including chlorophyll binding, photosynthesis, and thylakoid functions. Concurrently, the primary down-regulated GO pathways also retained ties to chloroplast functions. Furthermore, our investigation encompassed several defense-related genes (Figure 7F, S8). Notably, *PBZ1* (Kim et al., 2008), *OsNAC111* (Yokotani et al., 2014) and chloroplast immunity genes *LHCB5* (Liu et al., 2019) and *OsAPX8* (Jiang et al., 2016) exhibited positive involvement in *Pik-H4*-mediated immunity. In line with the findings presented in Figure S6, these results collectively suggest that *Pik-H4*-mediated effector-triggered immunity (ETI) is closely intertwined with chloroplast-related processes, indicating a potential role for *Pik-H4* in chloroplast immunity.

We extended our RNA-seq analysis to include OE-*Pik<sub>1</sub>-H4* /LTH and OE-*Pik<sub>2</sub>-H4-GFP* /LTH plants. The gene counts of up-regulated and down-regulated genes relative to LTH were 411 and 355, 2521 and 917, and 3357 and 1710 in *Pik-H4* NILs, OE-*Pik<sub>1</sub>-H4* /LTH, and OE-*Pik<sub>2</sub>-H4-GFP* /LTH, respectively (Figure 7D). Upon GO pathway enrichment analysis, overexpression of *Pik<sub>1</sub>-H4* or *Pik<sub>2</sub>-H4* resulted in down-regulation in pathways linked to defense response, heme binding, tetrapyrrole binding, and transcription regulator activity, while pathways associated with peroxidase activity, hydrolase activity, and molecular functions related to the cell skeleton were up-regulated (Figure S9B, C). Interestingly, most enriched pathways exhibited changes when *Pik<sub>1</sub>-H4* and *Pik<sub>2</sub>-H4* were co-expressed (Figure S9A), indicating the complex interplay between *Pik<sub>1</sub>-H4* and *Pik<sub>2</sub>-H4*. Zooming in on the subset of genes that were either up-regulated or down-regulated across the three types of plants (Figure 7D, red set: up-regulated; blue set: down-regulated), GO analysis revealed enrichment primarily in nucleotide binding, transferase activity, metabolic processes, and catalytic activity (Figure 7E). These pathways may be the potential mechanism of *Pik-H4* in the quiescent stage. A detailed analysis of immune-related genes unveiled that *Pik-H4*, acting as a singleton, reduced the expression of defense-related genes and transcription factors (TFs, with the exception of *OsWRKY13*) (Figure 7F, S8). However, four genes related to reactive oxygen species (ROS) were up-regulated, including two chloroplast immunity genes. This highlights the intricate nature of the regulatory network mediated by *Pik-H4*.

## Discussion

### The complexity in the long BDP mechanism

The TATA box is a fundamental promoter element within eukaryotes, which is crucial in initiating transcription for all three RNA polymerases. The canonical TATA box sequence is typically recognized as 5'-TATAWAW-3' (Kwak et al., 2013). However, a bidirectional TATA box (5'-TATATAT-3') has been identified to possess transcriptional capabilities in both directions, demonstrating heightened transcriptional activity (Xu, Thali and Schaffner, 1991). Analyzing split tests for BDPs lacks specific guiding principles. In this study, we employed the TATA box as a pivotal marker for segmenting the  $P_{Pik-H4}$ . The TATA box sequence at 462-469 bp in the *Pik-H4* promoter is a bidirectional TATA box, comprising two bidirectional TATA boxes situated on both the sense strand and the antisense strand, respectively (Figure 2E). Mutation of this segment resulted in a significant reduction in downstream gene expression on both sides of the promoter. Examining the promoter activity of a 100 bp sequence encompassing the integrated bidirectional TATA box, along with an adjacent bidirectional TATA box, revealed that the sequence indeed possessed bidirectional activity. Nevertheless, it could not fully restore the transcriptional activity of *Pik<sub>1</sub>-H4* and *Pik<sub>2</sub>-H4* in both directions back to the levels of NP (Figure 2D-F, BT1). Moreover, the recovery of expression intensity in downstream reporter genes was observed after adding the TSSs for both genes (Figure

2D-F, BT2), indicating that the 100 bp sequence primarily functions as a bidirectional regulatory element, with TSSs being indispensable for gene expression.

Transcriptional regulation is a complex process involving a multitude of factors, including TFBSs, *cis* elements, SNPs(Liu *et al.* , 2019), neighboring transcription units(Lee *et al.* , 2014) and various epigenetic modifications (Chen *et al.*, 2014). In contrast to the human genome, where approximately 67% of BDPs are shorter than 300 bp (Trinklein *et al.*, 2004), plant BDPs tend to be longer (Krom and Ramakrishna, 2008), introducing greater complexity to their regulatory mechanisms. Some reports on split BDPs focus on segments within 1500 bp (Banerjee *et al.*, 2013; Rao and Virupapuram, 2021), and identify crucial promoter regions that contribute to the basal expression of BDGs under specific experimental conditions. However, these studies often overlook the intricate *cis* regulatory elements for gene regulation or specificity. In our research, even by combining the minimal core promoter regions of *Pik<sub>1</sub>-H<sub>4</sub>* and *Pik<sub>2</sub>-H<sub>4</sub>* , we could not achieve BDP activity equivalent to NP levels (Figure 2A-C, B3). Intriguingly, this combination even increased GFP expression, indicating the intricate interplay of *cis* elements within  $P_{Pik-H_4}$  . Given that *Pik* BDPs encompass lengths of 2492 bp or 2542 bp, further assays to split and analyze promoters are necessary to unravel the underlying regulatory mechanisms of bidirectional NLR gene pairs. Unveiling the functionality of BDPs holds significant implications for synthetic biology, but it's evident that more extensive research is needed to understand these processes comprehensively.

### NLR gene pair *Pik<sub>1</sub>-H<sub>4</sub>* and *Pik<sub>2</sub>-H<sub>4</sub>* co-express in a BDG manner

NLR genes can be classified into singletons and pairs, depending on the number of genes involved in plant immunity. The Arabidopsis TNL gene pair *RRS1* and *SOC3* was reported to be organized in a BDG manner(Zhang *et al.* , 2017). It is well-known that the NLR gene pairs in the *Pik* locus are H2H genes. Despite this, there is limited knowledge about regulating NLR gene expression. In this study, we conducted a comprehensive analysis of the expression pattern of *Pik-H<sub>4</sub>* and found that under the regulatory control of  $P_{Pik-H_4}$  , *Pik-H<sub>4</sub>* exhibited significantly positive co-expression across various tissues. Furthermore, the infection caused by the rice blast fungus induced its expression in leaves and leaf sheaths. Based on these findings, we hypothesize that *Pik-H<sub>4</sub>* , functioning as a pair of resistance genes, maintains a basal expression level throughout the plant during the resting phase. This basal expression level acts as a surveillance system to detect the presence of effector proteins promptly, thereby initiating the disease resistance pathway upon pathogen invasion. Interestingly, while *Pikh-1* maintains constitutive transcription, *Pikh-2* is up-regulated in response to the rice blast fungus challenge(Zhai *et al.* , 2014). Identifying ten W-boxes in  $P_{Pik-H_4}$  (Figure 1A) highlights the significance of the W-box, a binding site for WRKY TFs, in pathogen-induced expression(In *et al.* , 2020). Notably, the observed divergence in expression between *Pik-H<sub>4</sub>* and *Pikh* might stem from differences in their BDP sequences (Figure S1). Furthermore, our investigation revealed robust promoter activity of *Pik-H<sub>4</sub>* within the vascular bundles of roots, stems, and leaf sheaths. One possible explanation for this pattern is that the hyphae of *M. oryzae* find a more accessible propagation route through vascular bundles, thereby necessitating heightened expression in these regions to provide a specific defense response. As a sensor protein, *Pik<sub>1</sub>-H<sub>4</sub>* exhibited an expression level approximately 0.6 times higher than that of *Pik<sub>2</sub>-H<sub>4</sub>*, and a noticeable divergence in expression was observed between the two at 24 hpi (Figure S4C). This finding was consistent with the results of promoter activity analyses following injection (Figure 4). Moreover, the appearance of rice blast fungus disrupted the linear expression relationship of *Pik-H<sub>4</sub>* (Figure 4J, K), suggesting that *M. oryzae* might stimulate *Pik-H<sub>4</sub>* expression in invaded and peripheral cells. This phenomenon prompts further exploration into the intricate mechanisms underlying signal transduction and NLR expression, which is vital for gaining deeper insights into the plant immune system's response to disease challenges.

It is well known that NLRs play a crucial role in triggering ROS production as part of the plant's defense response. For H2H NLR pairs, *Pikp* and *Pikh* are essential for initiating HR when confronted with the AvrPik effector(Zhai *et al.* , 2014; Zdrzałek *et al.* , 2020b). This mechanism contrasts with non-H2H NLR pairs like *Pigm* (Deng *et al.* , 2017) and *RGA4* / *RGA5* (Cesari, Kanzaki, *et al.* , 2014), which function differently regarding HR induction. We broke the expression relationship between *Pik<sub>1</sub>-H<sub>4</sub>* and *Pik<sub>2</sub>-H<sub>4</sub>*

under the control of  $P_{Pik-H4}$  by overexpressing one of them in  $Pik-H4$  NILs and expressing different ratios of  $Pik-H4$  in tobacco, the rice blast resistance and conductivity in ion leakage assays were not affected (Figure 5A, G). This intriguing result suggests that the expression levels of  $Pik-H4$  do not significantly influence the functional integrity of  $Pik_1-H4$  and  $Pik_2-H4$  proteins involved in immunity. It further indicates that the coordinated action of the  $Pik_1-H4/Pik_2-H4/AvrPik-E$  unit is sufficient to trigger HR, indicating the robustness of the plant's immune response machinery.

$Pik_1-H4$  and  $Pik_2-H4$  are organized in a BDG manner, functioning together to trigger rice blast resistance. This collaborative action is facilitated by the co-regulation of  $Pik-H4$  through bidirectional promoters, which are influenced by the presence of rice blast fungus *in planta*. Notably, a feedback regulatory mechanism exists between  $Pik_1-H4$  and  $Pik_2-H4$  (Figure 5E, F), further highlighting the intricate nature of their coordinated function. The gene structure of this BDG is well-suited to facilitate the controlled up-regulation of  $Pik-H4$  expression during immune responses, while also ensuring a consistent baseline expression in the absence of pathogen infection. This inherent readiness to counteract pathogens at any moment indicates the BDG structure's adaptive advantage in enhancing the plant's overall immune preparedness. Through the structure of BDG, NLR gene pairs establish a direct transcriptional regulatory link, which offers a more resource-efficient way to execute immune responses.

### Different roles of $Pik_1-H4$ and $Pik_2-H4$ as singletons and pair

Most of the NLR proteins are localized in the cytoplasm and nucleus. For instance, the *Arabidopsis* RPS4 (Heidrich *et al.*, 2011) and RRS1 (Deslandes *et al.*, 2003), rice  $Pikh-1/Pikh-2$  pair are localized in cytoplasm and nucleus (Zhai *et al.*, 2014), while the RGA4/RGA5 pair is cytoplasmic (Cesari, Kanzaki, *et al.*, 2014).  $Pik_1-H4$  and  $Pik_2-H4$  were observed to be localized in the plasma membrane and chloroplasts *in planta* (Figure 6A, E, Figure S6). Combined with the top enriched GO pathways at 24 hpi (Figure 7C), our results indicated that  $Pik$  genes might play roles in membrane and chloroplast immunity. Notably,  $Pik_1-H4$  as a singleton was found in vesicles around rice blast fungus, while  $Pik_2-H4$  singleton appeared in the nuclei of peripheral cells surrounding the infected cells (Figure 6D, H). The enrichment pathways of overexpression of singleton  $Pik-H4$  varied (Figure S9B, C). This suggests that the functions of the  $Pik-H4$  gene pair might involve distinct pathways when it comes to recognizing Avr proteins and inducing HR in response to the invasion of rice blast fungus (Figure 5G).

Singleton  $Pik_1-H4$  or  $Pik_2-H4$  promoted expression of ROS-related genes *OsRBOHB*, *OsRAC1*, *LHCB5* and *OsAPX8* (Figure 7F) but down-regulated defense response pathway (Figure S9B, C), defense-related genes *PR1a*, *PR1b*, *PR10* and *PBZ1* (Figure 7F), as well as multiple WRKY TFs (Table S2). Interestingly, when  $Pik_1-H4$  and  $Pik_2-H4$  are coupled together, no suppression of WRKY TFs was observed. Since both  $Pik_1-H4$  and  $Pik_2-H4$  are localized in the nucleus, it implies that  $Pik-H4$  may play a role in transcriptional regulation. Specifically,  $Pik_1-H4$  has been found to interact with the TF *OsBIHD1* and contribute to disease resistance (Liu *et al.*, 2017), although the precise function of  $Pik_2-H4$  in the nucleus is yet to be fully understood. The GO enrichment changes between 12 hpi and 24 hpi imply that  $Pik-H4$  functions in transcription during ETI (Figure 7B, C). The findings indicate that singleton  $Pik-H4$  is susceptible based on transcriptome profile. It is plausible that  $Pik-H4$  singletons or the pair may function as transcriptional cofactors, leading to transcriptional reprogramming in the context of immune responses.

## Materials and methods

### Motif analysis and sequence alignment

The motif analysis for promoters was performed with PlantRegMap (Tian *et al.*, 2020). The promoter sequences of  $Pik^*$  (Zhai *et al.*, 2011), *Pi1* (Hua *et al.*, 2012), *Pi7* (Campbell, Chen and Ronald, 2004), *Pikh* (Zhai *et al.*, 2014), *Pikm* (Ashikawa *et al.*, 2008), and *Pikp* (Zdrzałek *et al.*, 2020a) were collected as reported. Sequence alignment was performed with MAFFT (Rozewicki *et al.*, 2019) and was visualized with ESPript 3 (Robert and Gouet, 2014).

### Plasmid construction and rice transformation

To evaluate the  $P_{Pik-H4}$  activity, the promoter region of  $Pik-H4$  was cloned from  $Pik-H4$  NILs leaves with CTAB extraction and was inserted into a binary vector pGR $RFP::GFP$ . Then, the pGR vector was introduced into Nipponbare via *Agrobacterium*-mediated (EHA105) transformation. For promoter split and mutation assay, series plasmids were constructed with multi-fragment homologous recombination PCR. For GUS staining, P $P_{ik1-H4}$  and P $P_{ik2-H4}$  were cloned to pCAMBIA1305.1 and induced into Nipponbare. The coding sequences of  $P_{ik1-H4}$  and  $P_{ik2-H4}$  were inserted into the pOX- $GFP_{Ubi}::GFP$  vector and transformed into LTH or  $P_{ik-H4}$  NILs.  $P_{ik1-H4}$ ,  $P_{ik2-H4}$  and *AvrPik-E* coding sequences were cloned to pEAQ(Sainsbury, Thuenemann and Lomonosoff, 2009) with reconstruction: pEAQ-*FlagP<sub>35S</sub>::Flag*, pEAQ-*HAP<sub>35S</sub>::HA* and pEAQ-*MycP<sub>35S</sub>::Myc* respectively for tobacco transient expression.

### Plant materials and growth conditions

The rice cultivar Nip, rice blast susceptible cultivar LTH,  $P_{ik-H4}$  NILs in LTH background were used for constructing transgenic plants and inoculation assays. The  $RFP::P_{Pik-H4}::GFP$  /Nip, P $P_{ik1-H4}::GUS$ /Nip and P $P_{ik2-H4}::GUS$ /Nip were used for expression pattern analysis of  $P_{ik-H4}$ . The OE- $P_{ik1-H4}-GFP$  /*Pik* and OE- $P_{ik2-H4}-GFP$  /*Pik* were generated by crossing OE- $P_{ik1-H4}-GFP$  /LTH and OE- $P_{ik2-H4}-GFP$  /LTH with  $P_{ik-H4}$  NILs respectively. Nip was also used for protoplast transformation to identify bidirectional promoter activity. *Nicotiana benthamiana* was used for agroinfiltration to evaluate promoter activity and HR assays.

Rice cultivars grew on soil in a greenhouse with a natural light cycle and 30°C/light, 26°C/dark. Tobacco seeds were germinated in MS medium and transferred to the soil after germination in a growth chamber with a 16-h/8-h light/dark cycle at 24°C.

### *M. oryzae* materials and inoculation assay

The *M. oryzae* isolate GDYJ7 harboring *AvrPik-E* was used in this study. Spores were produced by growing the hypha in a complete medium with a 12-h/12-h light/dark cycle at 28°C for 10-14 days. Spray inoculation was performed as previously reported (Bonman, 1986) with modification to evaluate gene expression levels. Spores were collected with 0.02% Tween-20, and spore concentration was adjusted to  $5 \times 10^5$  spores/mL. The spore suspension was sprayed onto the surface of two-week-old rice seedling leaves evenly until visible droplets appeared with a spray gun. Samples were collected in 0, 6, 12, 24, 36, 48, 60, and 72 hpi after incubation in the dark for 12 h for quantitative real-time PCR (qRT-PCR). For phenotyping, leaves of 6- to 8-week-old seedlings were punch inoculated as described (Park *et al.*, 2012). Disease symptom was observed at 7 dpi. The lesion length was calculated using the software ImageJ. The sporulation rate on lesions was determined as described (Park *et al.*, 2012). Leaf sheath inoculation was performed as described (Koga *et al.*, 2004) with modification. In brief, the leaf sheaths of 2-week-old seedlings were carefully peeled. The spore suspension was adjusted to  $5 \times 10^5$  spores/mL and was injected with a syringe onto the inner surface of leaf sheaths. The seedlings were laid on a 20 cm plate with water and were grown with a 12-h/12-h light/dark cycle at 28°C for 7 days.

### Transient expression, promoter activity analysis and cell death assay in *N. benthamiana*

Expression vectors (pGR $RFP::P_{Pik-H4}::GFP$  and a series of pGR-based promoter split or mutation vectors, pEAQ P $_{35S}::P_{ik1-H4}::Flag$ , pEAQ P $_{35S}::P_{ik2-H4}::HA$ , pEAQ P $_{35S}::AvrPik-E::Myc$ ) were transformed into *Agrobacterium tumefaciens* GV3103. Each strain was set to  $OD_{600}=0.2$  and incubated in an induction buffer as described (Lapin *et al.*, 2019) in the dark at room temperature for 1 h. Then, the suspension was injected into 3- to 4-week-old tobacco leaves with a syringe. Data were collected after 2-3 days of infiltration. For promoter activity analysis, fifteen tobacco mesophyll cells from three seedlings were imaged with a confocal microscope (CarlZeiss LSM 750), and the fluorescence intensity was measured via the software ZEN. The excitation/emission wavelengths were 488 nm/490-560 nm for GFP, 543 nm/580-660 nm for RFP. Five 8-10 mm leaves with three biological replications were cut and put in tubes with 10 mL milliQ water for 30 min, then transferred to a new tube with 1 mL milliQ water at room temperature. Conductivity was measured at 0 h and 6 h with a conductivity meter (Lei-ci DDBJ-350).

## Rice protoplast isolation and transformation

Rice protoplast isolation from 1-week-old etiolated seedling sheaths and PEG-mediated transformation were performed as described (Zhang *et al.*, 2011). After incubation in the dark for 12-16 h at room temperature, the transformed rice protoplasts were observed with a confocal microscope.

## RNA extraction and qRT-PCR

Total RNA was extracted from inoculated leaves using TRIzol reagent (Invitrogen) following the manufacturer's protocol. RNA samples were reverse transcribed to cDNA (Vazyme HiScript III All-in-one RT SuperMix Perfect for qPCR). The qRT-PCR reaction systems were prepared as manufacturer's instruction (Vazyme AceQ Universal SYBR qPCR Master Mix) using a Real-Time PCR System (Applied Biosystems StepOnePlus). The  $2^{-\Delta\Delta C_t}$  method was used to evaluate the gene expression levels. The rice  $\beta\text{-actin}$  (*LOC-Os03g50885*) was used as the control gene and three biological repeats were performed for qRT-PCR. The results were visualized with Prism (v8.0.1) or ChiPlot (Xie *et al.*, 2023).

## Transcriptome profiling and statistical analysis

To elucidate the putative transcriptional function of *Pik-H4*, transcriptome profiling was performed by RNA-seq. For pathways analysis post-inoculation, three- to four-week-old LTH and *Pik-H4* NILs seedlings were spray inoculated with *M. oryzae* isolate GDYJ7 as previously described. Up to 0.1 g shoots were sampled at 0 (as mock treatment), 12 and 24 hpi. The inoculation assay was estimated by LTH phenotype 10 to 14 dpi. For singleton *Pik-H4* pathways analysis, three- to four-week-old OE-*Pik<sub>1</sub>-H4-GFP* / *Pik*, OE-*Pik<sub>2</sub>-H4-GFP* / *Pik* and *Pik-H4* NILs shoots were sampled. Total RNA was extracted using a Trizol reagent kit (Invitrogen) and the mRNA was enriched by the Oligo(dT) beads. Then, the enriched mRNA was fragmented into short fragments using fragmentation buffer and reversely transcribed into cDNA using NEBNext Ultra RNA Library Prep Kit for Illumina (New England Biolabs). The purified double-stranded cDNA fragments were end-repaired, A base added, and ligated to Illumina sequencing adapters. The ligation reaction was purified with the AMPure XP Beads(1.0X). And polymerase chain reaction (PCR) amplified. The resulting cDNA library was sequenced using Illumina Novaseq6000 by Gene Denovo Biotechnology Co. (Guangzhou, China). Differentially expressed genes (DEGs) were identified with  $P < 0.01$ ,  $|\log_2\text{Foldchange}| \geq 2$ . Correlation analysis was performed by R. Correlation of two parallel experiments provides the evaluation of the reliability of experimental results and operational stability. The correlation coefficient between two replicas was calculated to evaluate repeatability between samples. GO enrichment analysis was performed using TBtools (v1.120).

## ACKNOWLEDGEMENTS

This work was supported by the Natural Science Foundation of Guangdong Province, China (2019A1515011825, 2023A1515012101), the grant (CARS-01-18) from the National Rice Industry Technology System, China, and the National Key Research and Development Plan (2022YFD1200703), China.

## AUTHOR CONTRIBUTIONS

F.W.G., J.F.W., H.W. and T.G. designed the experiments. F.W.G. analyzed the data and wrote the manuscript. F.W.G., H.B.X., Q.W.H. and S.G. performed the experiments. All authors read and approved of the manuscript.

## DATA AVAILABILITY

Raw RNA-seq data have been deposited in the Sequence Read Archive of NCBI (<https://www.ncbi.nlm.nih.gov/sra>) under the accession PRJNA1013961.

## References

Ashikawa, I. *et al.* (2008) 'Two Adjacent Nucleotide-Binding Site-Leucine-Rich Repeat Class Genes Are Required to Confer Pikm-Specific Rice Blast Resistance', *Genetics*, 180(4), pp. 2267–2276. Available at: <https://doi.org/10.1534/genetics.108.095034>.

- Banerjee, J. *et al.* (2013) ‘An Intergenic Region Shared by At4g35985 and At4g35987 in Arabidopsis thaliana Is a Tissue Specific and Stress Inducible Bidirectional Promoter Analyzed in Transgenic Arabidopsis and Tobacco Plants’, *PLOS ONE* , 8(11), p. e79622. Available at: <https://doi.org/10.1371/journal.pone.0079622>.
- Bi, G. *et al.* (2021) ‘The ZAR1 resistosome is a calcium-permeable channel triggering plant immune signaling’, *Cell* , 184(13), pp. 3528–3541.e12. Available at: <https://doi.org/10.1016/j.cell.2021.05.003>.
- Campbell, M.A., Chen, D. and Ronald, P.C. (2004) ‘Development of Co-Dominant Amplified Polymorphic Sequence Markers in Rice that Flank the Magnaporthe grisea Resistance Gene Pi7(t) in Recombinant Inbred Line 29’, *Phytopathology*® , 94(3), pp. 302–307. Available at: <https://doi.org/10.1094/PHYTO.2004.94.3.302>.
- Cesari, S., Bernoux, M., *et al.* (2014) ‘A novel conserved mechanism for plant NLR protein pairs: the “integrated decoy” hypothesis’, *Frontiers in Plant Science* , 5. Available at: <https://www.frontiersin.org/articles/10.3389/fpls.2014.00606> (Accessed: 6 July 2023).
- Cesari, S., Kanzaki, H., *et al.* (2014) ‘The NB-LRR proteins RGA4 and RGA5 interact functionally and physically to confer disease resistance’, *The EMBO Journal* , 33(17), pp. 1941–1959. Available at: <https://doi.org/10.15252/embj.201487923>.
- Chen, Y. *et al.* (2014) ‘Transcriptional regulation and spatial interactions of head-to-head genes’, *BMC Genomics* , 15(1), p. 519. Available at: <https://doi.org/10.1186/1471-2164-15-519>.
- Deng, Y. *et al.* (2017) ‘Epigenetic regulation of antagonistic receptors confers rice blast resistance with yield balance’, *Science* , 355(6328), pp. 962–965. Available at: <https://doi.org/10.1126/science.aai8898>.
- Deslandes, L. *et al.* (2003) ‘Physical interaction between RRS1-R, a protein conferring resistance to bacterial wilt, and PopP2, a type III effector targeted to the plant nucleus’, *Proceedings of the National Academy of Sciences of the United States of America* , 100(13), pp. 8024–8029. Available at: <https://doi.org/10.1073/pnas.1230660100>.
- Fang, Y. *et al.* (2016) ‘Histone modifications facilitate the coexpression of bidirectional promoters in rice’, *BMC Genomics* , 17(1), p. 768. Available at: <https://doi.org/10.1186/s12864-016-3125-0>.
- Heidrich, K. *et al.* (2011) ‘Arabidopsis EDS1 connects pathogen effector recognition to cell compartment-specific immune responses’, *Science (New York, N.Y.)* , 334(6061), pp. 1401–1404. Available at: <https://doi.org/10.1126/science.1211641>.
- Hua, L. *et al.* (2012) ‘The isolation of Pi1, an allele at the Pik locus which confers broad spectrum resistance to rice blast’, *Theoretical and Applied Genetics* , 125(5), pp. 1047–1055. Available at: <https://doi.org/10.1007/s00122-012-1894-7>.
- In, S. *et al.* (2020) ‘Molecular Characterization of a Pathogen-Inducible Bidirectional Promoter from Hot Pepper (Capsicum annuum)’, *Molecular Plant-Microbe Interactions*® , 33(11), pp. 1330–1339. Available at: <https://doi.org/10.1094/MPMI-07-20-0183-R>.
- Jia, Y. *et al.* (2000) ‘Direct interaction of resistance gene and avirulence gene products confers rice blast resistance’, *The EMBO Journal* , 19(15), pp. 4004–4014. Available at: <https://doi.org/10.1093/emboj/19.15.4004>.
- Jiang, G. *et al.* (2016) ‘The rice thylakoid membrane-bound ascorbate peroxidase OsAPX8 functions in tolerance to bacterial blight’, *Scientific Reports* , 6(1), p. 26104. Available at: <https://doi.org/10.1038/srep26104>.
- Kim, S.T. *et al.* (2008) ‘Proteomics Analysis of Rice Lesion Mimic Mutant (spl1) Reveals Tightly Localized Probenazole-Induced Protein (PBZ1) in Cells Undergoing Programmed Cell Death’, *Journal of Proteome Research* , 7(4), pp. 1750–1760. Available at: <https://doi.org/10.1021/pr700878t>.
- Koga, H. *et al.* (2004) ‘A novel inoculation method of Magnaporthe grisea for cytological observation of the infection process using intact leaf sheaths of rice plants’, *Physiological and Molecular Plant Pathology* ,

64(2), pp. 67–72. Available at: <https://doi.org/10.1016/j.pmpp.2004.07.002>.

Krom, N. and Ramakrishna, W. (2008) ‘Comparative Analysis of Divergent and Convergent Gene Pairs and Their Expression Patterns in Rice, Arabidopsis, and Populus’, *Plant Physiology* , 147(4), pp. 1763–1773. Available at: <https://doi.org/10.1104/pp.108.122416>.

Kwak, H. *et al.* (2013) ‘Precise maps of RNA polymerase reveal how promoters direct initiation and pausing’, *Science (New York, N.Y.)* , 339(6122), pp. 950–953. Available at: <https://doi.org/10.1126/science.1229386>.

Lapin, D. *et al.* (2019) ‘A Coevolved EDS1-SAG101-NRG1 Module Mediates Cell Death Signaling by TIR-Domain Immune Receptors’, *The Plant Cell* , 31(10), pp. 2430–2455. Available at: <https://doi.org/10.1105/tpc.19.00118>.

Lee, T.J. *et al.* (2014) ‘Suppression of Expression Between Adjacent Genes Within Heterologous Modules in Yeast’, *G3 Genes|Genomes|Genetics* , 4(1), pp. 109–116. Available at: <https://doi.org/10.1534/g3.113.007922>.

Lijavetzky, D., Carbonero, P. and Vicente-Carbajosa, J. (2003) ‘Genome-wide comparative phylogenetic analysis of the rice and Arabidopsis Dof gene families’, *BMC evolutionary biology* , 3, p. 17. Available at: <https://doi.org/10.1186/1471-2148-3-17>.

Liu, H. *et al.* (2017) ‘NBS-LRR protein Pik-H4 Interacts with OsBIHD1 to Balance Rice Blast Resistance and Growth by coordinating Ethylene-Brassinosteroid pathway’, *Frontiers in Plant Science* , 8. Available at: <https://www.frontiersin.org/articles/10.3389/fpls.2017.00127> (Accessed: 21 July 2023).

Liu, M. *et al.* (2019) ‘Phosphorylation-guarded light-harvesting complex II contributes to broad-spectrum blast resistance in rice’, *Proceedings of the National Academy of Sciences* , 116(35), pp. 17572–17577. Available at: <https://doi.org/10.1073/pnas.1905123116>.

Liu, X. *et al.* (2014) ‘Identification and functional characterization of bidirectional gene pairs and their intergenic regions in maize’, *BMC Genomics* , 15(1), p. 338. Available at: <https://doi.org/10.1186/1471-2164-15-338>.

Ma, S. *et al.* (2020) ‘Direct pathogen-induced assembly of an NLR immune receptor complex to form a holoenzyme’, *Science* , 370(6521), p. eabe3069. Available at: <https://doi.org/10.1126/science.abe3069>.

Mackey, D. *et al.* (2002) ‘RIN4 Interacts with Pseudomonas syringae Type III Effector Molecules and Is Required for RPM1-Mediated Resistance in Arabidopsis’, *Cell* , 108(6), pp. 743–754. Available at: [https://doi.org/10.1016/S0092-8674\(02\)00661-X](https://doi.org/10.1016/S0092-8674(02)00661-X).

Martin, R. *et al.* (2020) ‘Structure of the activated ROQ1 resistosome directly recognizing the pathogen effector XopQ’, *Science* , 370(6521), p. eabd9993. Available at: <https://doi.org/10.1126/science.abd9993>.

Meng, F. *et al.* (2021) ‘Analysis of natural variation of the rice blast resistance gene Pike and identification of a novel allele Pikg’, *Molecular Genetics and Genomics* , 296(4), pp. 939–952. Available at: <https://doi.org/10.1007/s00438-021-01795-w>.

Nakano, T. *et al.* (2006) ‘Genome-wide analysis of the ERF gene family in Arabidopsis and rice’, *Plant Physiology* , 140(2), pp. 411–432. Available at: <https://doi.org/10.1104/pp.105.073783>.

Park, C.-H. *et al.* (2012) ‘The Magnaporthe oryzae Effector AvrPiz-t Targets the RING E3 Ubiquitin Ligase APIP6 to Suppress Pathogen-Associated Molecular Pattern-Triggered Immunity in Rice’, *The Plant Cell* , 24(11), pp. 4748–4762. Available at: <https://doi.org/10.1105/tpc.112.105429>.

Rao, V. and Virupapuram, V. (2021) ‘Identification and characterization of a biphasic/bidirectional wound-inducible RHA3B gene promoter from Arabidopsis thaliana’. bioRxiv, p. 2021.01.28.428589. Available at: <https://doi.org/10.1101/2021.01.28.428589>.

- Ray, S. *et al.* (2016) ‘Analysis of Magnaporthe oryzae Genome Reveals a Fungal Effector, Which Is Able to Induce Resistance Response in Transgenic Rice Line Containing Resistance Gene, Pi54’, *Frontiers in Plant Science* , 7. Available at: <https://www.frontiersin.org/articles/10.3389/fpls.2016.01140> (Accessed: 31 July 2023).
- Robert, X. and Gouet, P. (2014) ‘Deciphering key features in protein structures with the new ENDscript server’, *Nucleic Acids Research* , 42(Web Server issue), pp. W320-324. Available at: <https://doi.org/10.1093/nar/gku316>.
- Rozewicki, J. *et al.* (2019) ‘MAFFT-DASH: integrated protein sequence and structural alignment’, *Nucleic Acids Research* , 47(W1), pp. W5–W10. Available at: <https://doi.org/10.1093/nar/gkz342>.
- Sainsbury, F., Thuenemann, E.C. and Lomonosoff, G.P. (2009) ‘pEAQ: versatile expression vectors for easy and quick transient expression of heterologous proteins in plants’, *Plant Biotechnology Journal* , 7(7), pp. 682–693. Available at: <https://doi.org/10.1111/j.1467-7652.2009.00434.x>.
- Tian, F. *et al.* (2020) ‘PlantRegMap: charting functional regulatory maps in plants’, *Nucleic Acids Research* , 48(D1), pp. D1104–D1113. Available at: <https://doi.org/10.1093/nar/gkz1020>.
- Trinklein, N.D. *et al.* (2004) ‘An Abundance of Bidirectional Promoters in the Human Genome’, *Genome Research* , 14(1), pp. 62–66. Available at: <https://doi.org/10.1101/gr.1982804>.
- Wang, G. *et al.* (2015) ‘The Decoy Substrate of a Pathogen Effector and a Pseudokinase Specify Pathogen-Induced Modified-Self Recognition and Immunity in Plants’, *Cell Host & Microbe* , 18(3), pp. 285–295. Available at: <https://doi.org/10.1016/j.chom.2015.08.004>.
- Wang, Jizong *et al.* (2019) ‘Reconstitution and structure of a plant NLR resistosome conferring immunity’, *Science* , 364(6435), p. eaav5870. Available at: <https://doi.org/10.1126/science.aav5870>.
- Whitehall, S.K., Kassavetis, G.A. and Geiduschek, E.P. (1995) ‘The symmetry of the yeast U6 RNA gene’s TATA box and the orientation of the TATA-binding protein in yeast TFIIB.’, *Genes & Development* , 9(23), pp. 2974–2985. Available at: <https://doi.org/10.1101/gad.9.23.2974>.
- Williams, E.J.B. and Bowles, D.J. (2004) ‘Coexpression of Neighboring Genes in the Genome of Arabidopsis thaliana’, *Genome Research* , 14(6), pp. 1060–1067. Available at: <https://doi.org/10.1101/gr.2131104>.
- Williams, S.J. *et al.* (2014) ‘Structural Basis for Assembly and Function of a Heterodimeric Plant Immune Receptor’, *Science* , 344(6181), pp. 299–303. Available at: <https://doi.org/10.1126/science.1247357>.
- Xiao, W. *et al.* (2011) ‘Identification and fine mapping of a resistance gene to Magnaporthe oryzae in a space-induced rice mutant’, *Molecular Breeding* , 28(3), pp. 303–312. Available at: <https://doi.org/10.1007/s11032-010-9481-6>.
- Xie, J. *et al.* (2023) ‘Tree Visualization By One Table (tvBOT): a web application for visualizing, modifying and annotating phylogenetic trees’, *Nucleic Acids Research* , 51(W1), pp. W587–W592. Available at: <https://doi.org/10.1093/nar/gkad359>.
- Xie, Y. *et al.* (2022) ‘SH3P2, an SH3 domain-containing protein that interacts with both Pib and Avr-Pib, suppresses effector-triggered, Pib-mediated immunity in rice’, *Molecular Plant* , 15(12), pp. 1931–1946. Available at: <https://doi.org/10.1016/j.molp.2022.10.022>.
- Xu, L.C., Thali, M. and Schaffner, W. (1991) ‘Upstream box/TATA box order is the major determinant of the direction of transcription.’, *Nucleic Acids Research* , 19(24), pp. 6699–6704.
- Yan, X. and Talbot, N.J. (2016) ‘Investigating the cell biology of plant infection by the rice blast fungus Magnaporthe oryzae’, *Current Opinion in Microbiology* , 34, pp. 147–153. Available at: <https://doi.org/10.1016/j.mib.2016.10.001>.

Yokotani, N. *et al.* (2014) ‘OsNAC111, a Blast Disease–Responsive Transcription Factor in Rice, Positively Regulates the Expression of Defense-Related Genes’, *Molecular Plant-Microbe Interactions*<sup>®</sup>, 27(10), pp. 1027–1034. Available at: <https://doi.org/10.1094/MPMI-03-14-0065-R>.

Zdrzałek, R. *et al.* (2020a) ‘The rice NLR pair Pikip-1/Pikip-2 initiates cell death through receptor cooperation rather than negative regulation’, *PLOS ONE*, 15(9), p. e0238616. Available at: <https://doi.org/10.1371/journal.pone.0238616>.

Zdrzałek, R. *et al.* (2020b) ‘The rice NLR pair Pikip-1/Pikip-2 initiates cell death through receptor cooperation rather than negative regulation’, *PLOS ONE*, 15(9), p. e0238616. Available at: <https://doi.org/10.1371/journal.pone.0238616>.

Zhai, C. *et al.* (2011) ‘The isolation and characterization of Pik, a rice blast resistance gene which emerged after rice domestication’, *New Phytologist*, 189(1), pp. 321–334. Available at: <https://doi.org/10.1111/j.1469-8137.2010.03462.x>.

Zhai, C. *et al.* (2014) ‘Function and Interaction of the Coupled Genes Responsible for Pik-h Encoded Rice Blast Resistance’, *PLOS ONE*, 9(6), p. e98067. Available at: <https://doi.org/10.1371/journal.pone.0098067>.

Zhang, Y. *et al.* (2011) ‘A highly efficient rice green tissue protoplast system for transient gene expression and studying light/chloroplast-related processes’, *Plant Methods*, 7(1), p. 30. Available at: <https://doi.org/10.1186/1746-4811-7-30>.

Zhang, Y. *et al.* (2017) ‘Temperature-dependent autoimmunity mediated by chs1 requires its neighboring TNL gene SOC3’, *The New Phytologist*, 213(3), pp. 1330–1345. Available at: <https://doi.org/10.1111/nph.14216>.

Zhao, Y.-B. *et al.* (2022) ‘Pathogen effector AvrSr35 triggers Sr35 resistosome assembly via a direct recognition mechanism’, *Science Advances*, 8(36), p. eabq5108. Available at: <https://doi.org/10.1126/sciadv.abq5108>.

### Figure legends

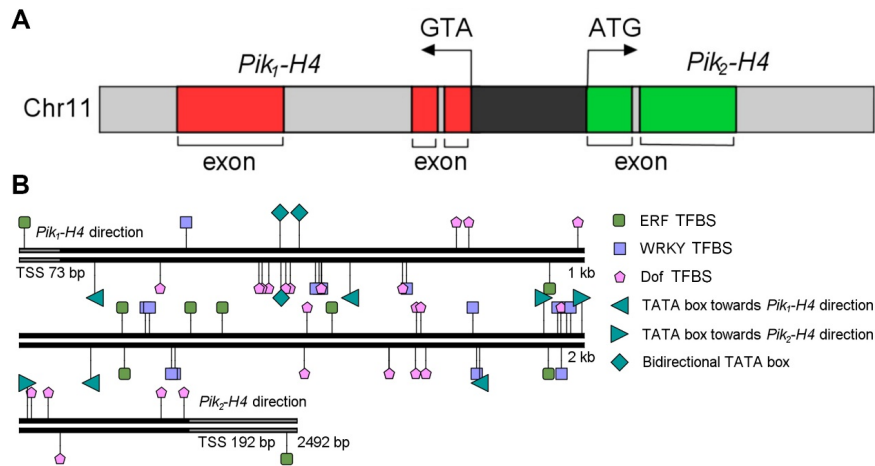


Figure 1. The structure of the *Pik-H<sub>4</sub>* gene and promoter region

(A) The schematic structure of *Pik<sub>1</sub>-H<sub>4</sub>* and *Pik<sub>2</sub>-H<sub>4</sub>* in rice chromosome 11. (B) TATA boxes and defense-related TFBSs in *P<sub>Pik-H<sub>4</sub></sub>*. The motif analysis for promoters was performed with PlantRegMap.

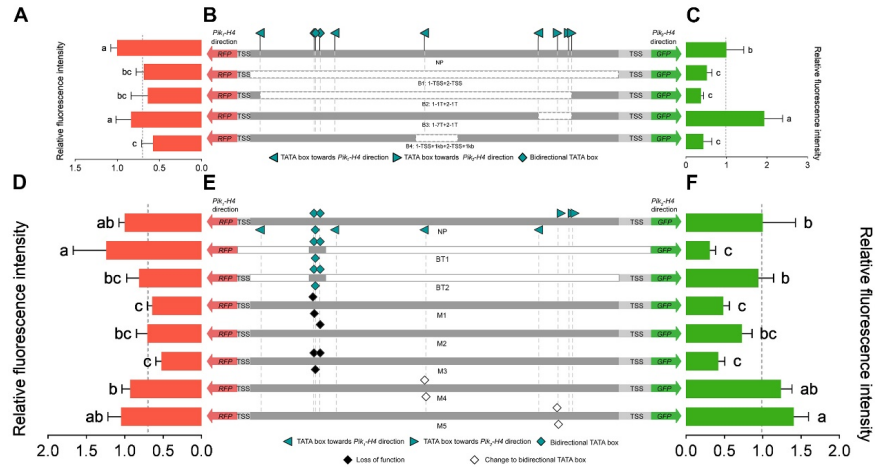


Figure 2. Promoter analysis of different  $P_{Pik-H4}$  sequences

(A - C) Minimal promoter region of  $P_{Pik-H4}$ . The schematic of a combination of two directions is shown in (B). (D - F) Mutation of bidirectional TATA boxes. The schematic is shown in (B). Data represent means  $\pm$  standard deviation (n=10). The RFP and GFP relative fluorescence intensity compared to the native promoter was shown in (G), (I), (G) and (I). The lowercase letters (a, b, c) indicate the data were at  $P < 0.01$  level according to one-way ANOVA with Dunnett's test. The dashed lines represent the value of the empty RFP :: GFP plasmid.

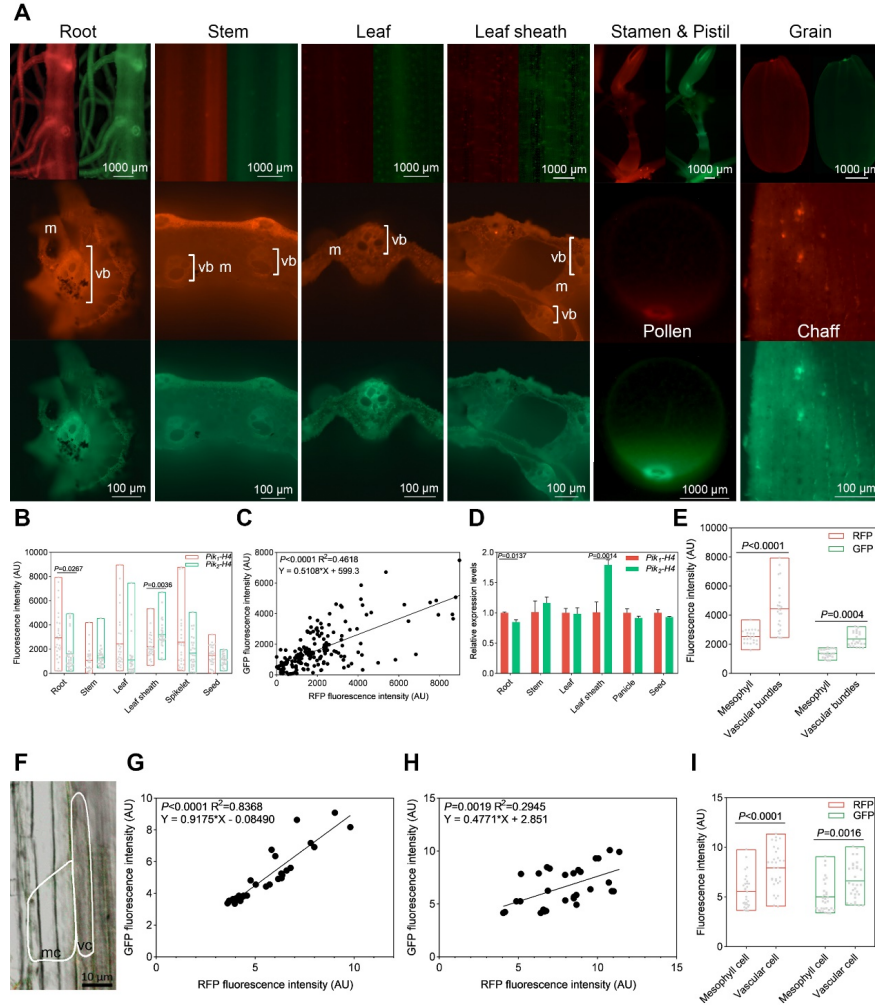


Figure 3. *Pik-H4* co-expressed in tissues and cells

(A) The fluorescence microscopy of  $RFP::P_{Pik_1-H4}::GFP$  /Nip plants. The RFP and GFP signals represent the promoter activity of  $Pik_1-H4$  and  $Pik_2-H4$  respectively. The letter “m” represents mesophyll tissue, and “vb” represents vascular bundles. (B, E and I) Measurement of fluorescence intensity. (B and E) were measured from (A), (I) was measured from (F). One-way ANOVA with student’s *t*-test,  $n=30$ . (C, G and H) The linear regression of RFP and GFP signals. The F-test was employed to compare statistical models applied to a dataset through linear regression. (C) was built from (A),  $n=180$ . (G and H) were constructed from (F),  $n=30$ . (D) Relative expression levels of  $Pik_1-H4$  and  $Pik_2-H4$ . Data represent means  $\pm$  standard deviation (One-way ANOVA with student’s *t*-test,  $n=3$ ). (F) The confocal fluorescence microscopy. The letter “mc” represents mesophyll cell, and “vc” represents vascular cell.

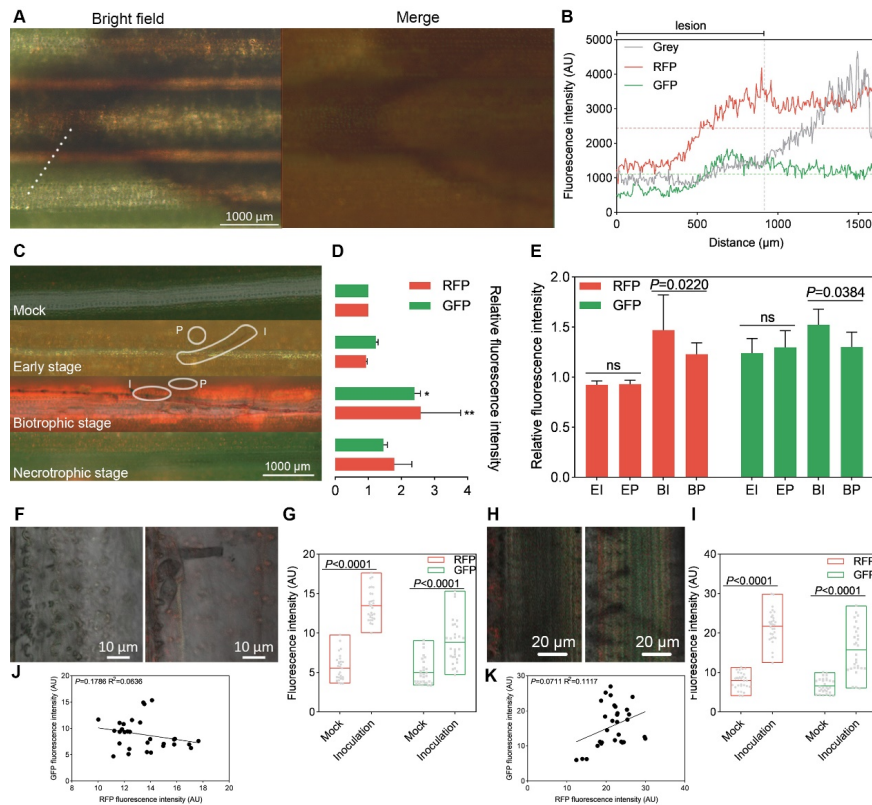


Figure 4.  $P_{Pik-H4}$  activity was up-regulated after infection in  $RFP::P_{Pik-H4}::GFP$  /Nip plants

(A and B) The promoter activity upon infection in leaf tissue. The fluorescence intensity in (B) was measured along the dotted line from (A). The red and green dashed lines represent the average RFP and GFP intensity in a normal state in leaves. The grey line was measured in the bright field and indicated the lesion area when the values were lower. (C - E) The promoter activity upon infection in the leaf vascular bundle. (D and E) The relative fluorescence intensity compared to the mock treatment from (C). Data represent means  $\pm$  standard deviation (One-way ANOVA with student's  $t$ -test,  $n=10$ ). One asterisk indicates  $P < 0.05$ , two asterisks indicate  $P < 0.01$ . I, infected area. P, peripheral area of the infected area. E, early stage of infection. B, biotrophic stage. (F - K) The confocal fluorescence microscopy in leaf sheaths. (F, G and J), mesophyll cell. (H, I and K), vascular bundles. (G and I), One-way ANOVA with student's  $t$ -test,  $n=10$ . (J and K) The linear regression from (F and H), The F-test was employed to compare statistical models applied to a dataset through linear regression,  $n=10$ .

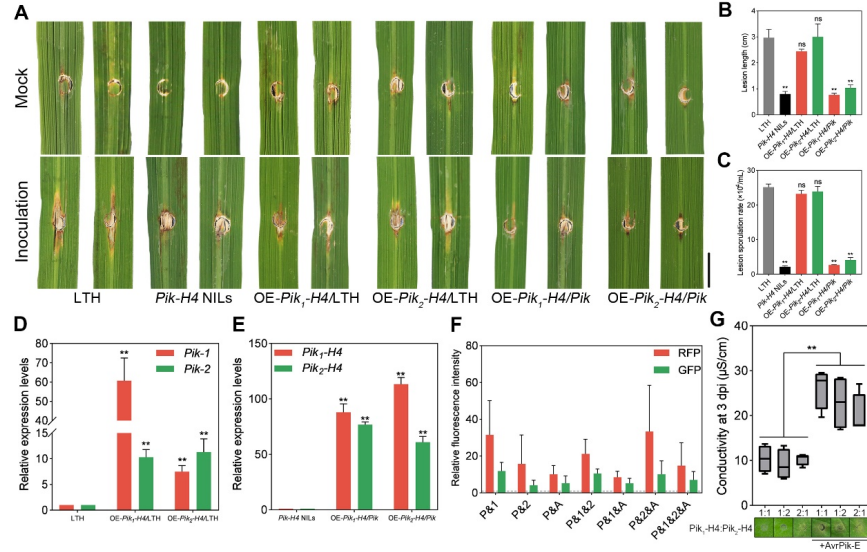


Figure 5. Different *Pik-H4* expressions facing the rice blast fungus or effector

(A) Punch inoculation in different plants overexpressing *Pik<sub>1</sub>-H4* or *Pik<sub>2</sub>-H4*. Bar=1 cm. (B and C) Measurement of lesion length and sporulation rate from (A). Data represent means  $\pm$  standard deviation, One asterisk indicates  $P < 0.05$ , two asterisks indicate  $P < 0.01$  (One-way ANOVA with student's *t*-test,  $n=5$ ). (D and E) The relative expression levels measured by qRT-PCR of *Pik* genes from uninfected plants in (A). Data represent means  $\pm$  standard deviation, One asterisk indicates  $P < 0.05$ , two asterisks indicate  $P < 0.01$  (One-way ANOVA with student's *t*-test,  $n=3$ ). (F) Relative fluorescence intensity compared to the *RFP* :: *P<sub>Pik-H4</sub>* :: *GFP* (P) plasmid in tobacco transient assays,  $n=10$ . 1, *P<sub>35S</sub>* :: *Pik<sub>1</sub>-H4* :: *Flag*. 2, *P<sub>35S</sub>* :: *Pik<sub>2</sub>-H4* :: *Ha*. A, *P<sub>35S</sub>* :: *AvrPik-E* :: *Myb*. The dashed line represents intensity value=1. (G) Ion leakage assay measuring *Pik-H4*-mediated cell death in tobacco at 3 dpi. The *Agrobacteria* expressing *Pik<sub>1</sub>-H4-Flag* and *Pik<sub>2</sub>-H4-HA* were mixed in different volumes with or without *AvrPik-E-Myc*. Two asterisks indicate  $P < 0.01$  (One-way ANOVA with student's *t*-test,  $n=5$ ).

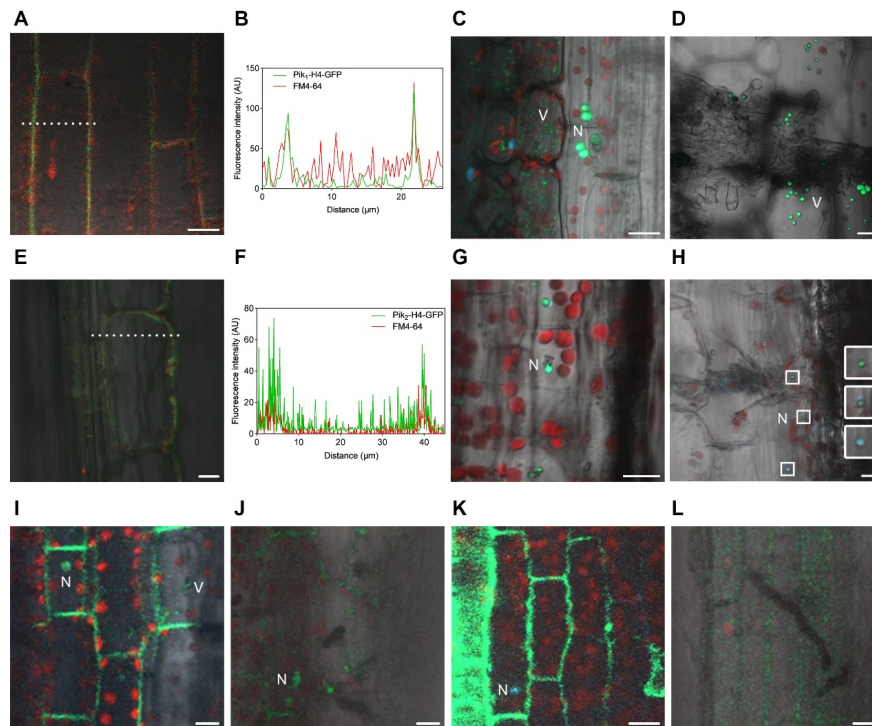


Figure 6. Subcellular location of Pik<sub>1</sub>-H4 and Pik<sub>2</sub>-H4 in leaf sheaths *in planta*

(A - D ) Overexpression of *Pik<sub>1</sub>-H4-GFP* in LTH. (A ) Pik<sub>1</sub>-H4-GFP was in the membrane and cytosol. (B ) Fluorescence intensity of Pik<sub>1</sub>-H4-GFP and membrane dye FM4-64 along the dotted line in (A ). (C ) Pik<sub>1</sub>-H4-GFP was in the nucleus and vesicles. (D ) Pik<sub>1</sub>-H4-GFP was in vesicles when infected. (E - H ) Overexpression of *Pik<sub>2</sub>-H4-GFP* in LTH. (E ) Pik<sub>2</sub>-H4-GFP was in the membrane and cytosol. (F ) Fluorescence intensity of Pik<sub>2</sub>-H4-GFP and membrane dye FM4-64 along the dotted line in (E ). (G ) Pik<sub>2</sub>-H4-GFP was in nucleus. (H ) Pik<sub>2</sub>-H4-GFP was in the nucleus when infected. (I and J ) Overexpression of *Pik<sub>1</sub>-H4-GFP* in *Pik-H4* NILs. (I ) Pik<sub>1</sub>-H4-GFP was in the membrane, cytosol, nucleus and vesicles. (K and L ) Overexpression of *Pik<sub>2</sub>-H4-GFP* in *Pik-H4* NILs. (K ) Pik<sub>2</sub>-H4-GFP was in the membrane, cytosol and nucleus. (J and L ) Pik<sub>1</sub>-H4-GFP and Pik<sub>2</sub>-H4-GFP signals were weakened when infected with *M. oryzae* in *Pik-H4* NILs. FM4-64 was marked in red in (A and E ). In (C , D , G ,H , I - L ), chlorophyll A was marked in red and the nucleus was dyed with DAPI (blue). All the bars represent 10 μm.

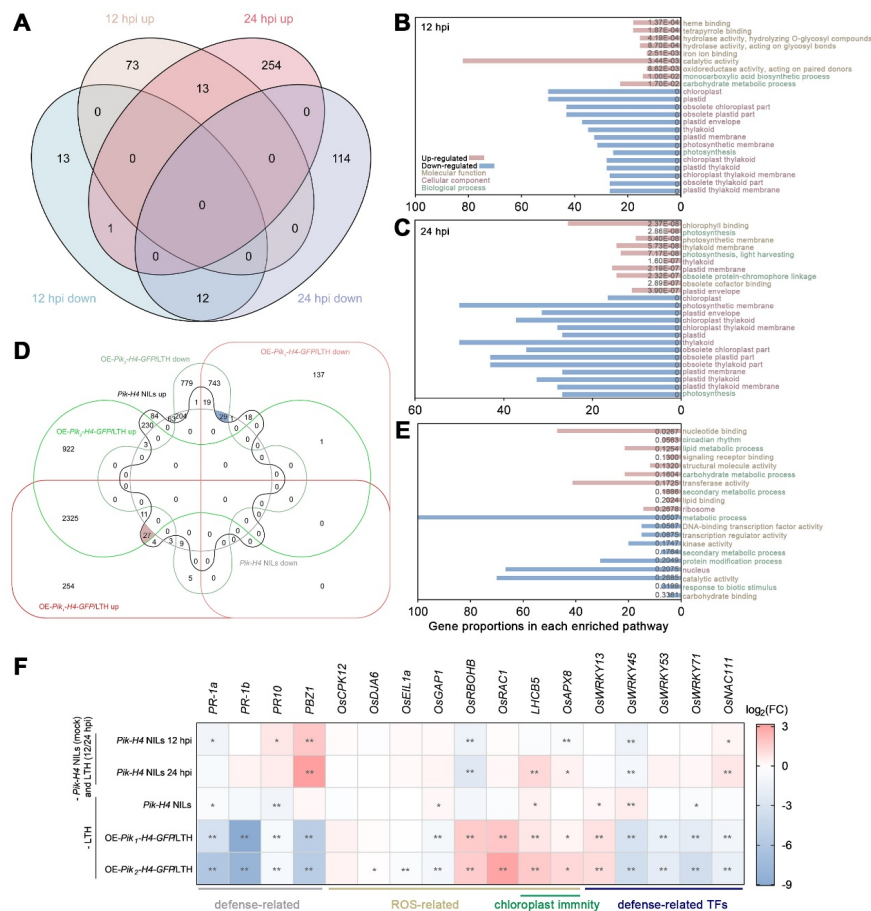


Figure 7. Transcriptome profiling analysis of different *Pik-H4* plants

(A) Venn diagram of DEGs in *Pik-H4* NILs after inoculation (Filtered *Pik-H4* NILs mock groups and corresponding LTH treatment groups). For all transcriptome analysis,  $\log_2\text{Foldchange(FC)} \geq 2$ ,  $P < 0.01$ . (B and C) GO pathway enrichments of DEGs in 12 and 24 hpi respectively. In (B, C and E), the x axis indicates the gene proportions in each enriched pathway; the numbers in the plots represent the  $P$  values of each pathway within all genes in the corresponding pathways; the up-/down-regulated pathways are shaded in pink and light-blue; the enrichment was clustered in three top GO groups and marked in different colors (Molecular function, brown. Cellular component, purple-red. Biological process, celadon). (D) Venn diagram of DEGs in *Pik-H4* NILs, OE-*Pik*<sub>1</sub>-*H4*-GFP/LTH and OE-*Pik*<sub>2</sub>-*H4*-GFP/LTH (Filtered LTH groups). The set shaded in pink or light blue represents the intersection of up- or down-regulated DEGs of *Pik-H4* NILs, OE-*Pik*<sub>1</sub>-*H4*-GFP/LTH and OE-*Pik*<sub>2</sub>-*H4*-GFP/LTH. (E) GO pathway enrichments of DEGs in *Pik-H4* NILs, OE-*Pik*<sub>1</sub>-*H4*-GFP/LTH and OE-*Pik*<sub>2</sub>-*H4*-GFP/LTH. (F) Fold change analysis of immune-related genes in different transcriptome profiles (One asterisk indicates  $P < 0.05$ , two asterisks indicate  $P < 0.01$ ).

### Hosted file

Supplementary Figure.docx available at <https://authorea.com/users/665126/articles/666541-co-expression-and-function-of-head-to-head-nlr-gene-pair-pik-h4>

### Hosted file

Supplementary Table.docx available at <https://authorea.com/users/665126/articles/666541-co-expression-and-function-of-head-to-head-nlr-gene-pair-pik-h4>